HHS Public Access

Author manuscript

J Mater Res Technol. Author manuscript; available in PMC 2022 July 27.

Published in final edited form as:

J Mater Res Technol. 2021 ; 15: 6356–6366. doi:10.1016/j.jmrt.2021.11.048.

An investigation into the polylactic acid texturization through thermomechanical processing and the improved d_{33} piezoelectric outcome of the fabricated scaffolds

Amirhossein Farahani[a], **Abbas Zarei-Hanzaki**[a,**], **Hamid Reza Abedi**[b,*], **Ismaeil Haririan**[c], **Mohammad Akrami**[c], **Zeynab Aalipour**[a], **Lobat Tayebi**[d]

[a]Hot Deformation & Thermomechanical Processing Laboratory of High Performance Engineering Materials, School of Metallurgy and Materials Engineering, College of Engineering, University of Tehran, Tehran, Iran

[b]School of Metallurgy & Materials Engineering, Iran University of Science and Technology (IUST), Tehran, Iran

[c]Department of Pharmaceutical Biomaterials, And Medical Biomaterials Research Center, Faculty of Pharmacy, Tehran University of Medical Sciences, Tehran, Iran

[d]School of Dentistry, Marquette University, Milwaukee, WI, 53233, USA

Abstract

The bio/sensors performance has been established to be significantly affected through partially or entirely alignment of nano/microfibrous in polymeric mats. The matter of crystalline/amorphous proportion in semicrystalline polymers is another factor that can affect the application of the piezoelectric patches. The present work deals with fabricating the scaffolds of micro/nanofibers through a modified electrospinning procedure. The ratio of the relevant organic and polar solvents, the beading, the degree of fiber alignment, and fiber thickness have been intentionally elaborated. An unaligned unbeaded nanofibrous mat has been fabricated after tuning the solvents to poly-lactic acid ratio. This paper, for the first time, deals with the calculation of the value of d_{33} value of a commercial PLA and its improvement, it has been revealed that the d_{33} piezoelectric property is improved as a consequence of the thermo-mechanical processing above the cold crystallization temperature. The applied thermo (mechanical) processing causes the structural evolution from amorphous to crystallized states. Formation of the α and α' crystalline phases is introduced as the main responsible for the improvement of the piezoelectric property. This improvement not only is correlated with the degree of crystallinity, but also the orientation and alignment of the crystallites is known to be influential. In this respect, the complex helical chain structural evolution of poly-lactic acid has been analyzed through Herman's orientation function. It has been found that, besides the characterized disorder-to-order phase transformation, the C=O branched out dipoles interactions significantly affects by the texturization of the aligned polymeric chains in the direction of the electrospinning which is known as the main factor to promote the piezoelectric property of processed mat.

*Corresponding author. habedi@iust.ac.ir (H.R. Abedi). **Corresponding author. zareih@ut.ac.ir (A. Zarei-Hanzaki).

Keywords

Piezoelectric; Poly-lactic acid; Thermomechanical processing; Electrospinning; Crystallinity; Texturization

1. Introduction

Considering the electroactive biopolymers following the potential to transduce mechanical and electrical energy, Poly-Lactic Acid (PLA) has drawn the researchers' attention. This is attributed to the non-centrosymmetric complex structure of PLA, as a Food and Drug Administration (FDA)-approved polymer, which has the potential to be studied in the course of piezoelectricity [1,2]. An individual chain, in polymer structure, may be non-centrosymmetric, but the amorphous network will be highly isotropic, which diminishes the probability of piezoelectricity. Interestingly, this type of centrosymmetric has been removed in amorphous PLA; therefore, the PLA shows piezoelectricity even in its non-crystalline state [3,4].

It has been proved that crystallization would improve the non-centrosymmetric structure. Among the 32 crystallographic point groups, 21 of them do not possess inversion symmetry which are the crystalline state of the polymers [2]. PLA crystallizes into four distinct phases, among them α’ with pseudo hexagonal unit cell and α with an orthorhombic crystalline structure [5]. Achieving an utterly crystallized structure is impossible in polymers; in the meanwhile of crystallization, crystalline regions will grow within the amorphous matrix, and on average, these crystallites will exhibit a randomly oriented distribution [6,7].

Among the various procedures improving the non-centrosymmetric structure, stretching is a common method [8]. Polymers possessing handedness, those with helical conformation as a consequence of chiral monomer units, can contain a mirror plane perpendicular to its drawing axis, and thus because of the breaking of the mirror plane by the helical twist, the piezoelectricity can be improved [9]. Another promising method which can be used to promote the anisotropy is electrical poling, through which a large tendency of dipole alignment is achieved within the structure. This is only applicable in the case of ferroelectric materials where the polarization is spontaneous and reversible [10]. Piezoelectricity defines as the physical properties of the materials containing the dipole groups which do not cancel each other within the microstructure of the complex material's structure. There are many PE constants regarding the type of normal or shear piezoelectricity and direct or diverse piezoelectricity; in order to provide an appropriate portrayal to them, Fig. 1 is presented.

There are two diverse types of piezoelectricity; Normal and shear. Normal PE assigns to the materials that react to the employed force straightly. When the structure deforms in X, Y, or Z directions, the electrical charge concentrates on one of the suggested directions of the specimen. When an excitation charge employs the unit, volume growth appears in the same way. The shear piezoelectricity issues into the statement in materials that twist the sample in acknowledgment of the electrical stimulation [11].

Stretching the polymer adjusts the amorphous strands in the film/fiber plane and promotes uniform rotation of the crystallites by an electric field. Depending on whether stretching is uniaxial or biaxial, the electrical and mechanical properties are either highly anisotropic or isotropic in the plane of the polymer sheet. Polymer poling can be accomplished using a direct contact method or a corona discharge. In this fashion, one of the favorite techniques is ES. During the ES process, speedy solvent drying constitutes an amorphous structure of oriented fibers; increasing the crystallinity is more comfortable by the secondary hot drawing process. By diminishing the fiber diameter, more surface area is achieved, and thus, the glass transition and melt temperature inconsiderably wane [12].

In the case of PLA, the d_{14} PE constant has been studied chiefly, and it has been demonstrated that the order of constant ranges between 9 and 11 pc/N [13,14]. In comparison, post-treatment such as annealing or further thermomechanical process has the potential to increase this PE constant approximately near to 20 pc/N [15]. There is a huge lack of knowledge around the calculation of the PLA PE d_{33} constant and its fluctuation as a result of the thermo-mechanical process.

The most well-known PLA PE constant is defined as d_{14}. Throughout the experimental measurements of research from Occhiai et al. on 0-cut PLLA, carrying side along z-axis which also was their elongation axis, samples manifested these cases had a d_{14} PE coefficient equal to 9.82 pC/N [16].

The piezoelectricity not only is sensitive to the glassy transition behavior, but also is a function of crystalline/amorphous structure characteristics. It has been [17] illustrated that the amorphous region will contribute to the piezoelectricity just if the molecular chains follow some degree of alignment at least. On the one hand, chirality and helical PLA conformation provide a proper condition for the presence of piezoelectricity even in the absence of any further processing; thus, simply aligning the polymer chains is sufficient to remove any centrosymmetric and permit piezoelectricity [18]. In this respect, the thermo-mechanical processing is highly capable to change the alignment of polymeric chains accommodating the applied stress. This significantly reorganizes the crystalline regions embedded within the amorphous matrix and improves the non-centrosymmetric structure.

As a semicrystalline polymer, the crystallization process and crystal structure of PLA have been studied by various groups. PLA has the potential to experience four kinds of crystal modification, where α, α', β, and γ phases are formed under the different preparation process [19-22]. The most thermodynamically stable phase, α form, has a 10_3 helical chain conformation [23] which can crystallize from melt or solution and mainly differentiate from the α′ form. The α′ form crystallizes at temperatures below 120 ° C and is known to be the disorder form of α, while the α form achieves above this disorder to order transformation temperature [19].

In another opinion, PLA is not classified as a ferroelectric material, and uniaxial arrangement would serve sufficient to compromise its natural piezo-response. Therefore, because of the original PE characteristics of the PLA, no additional fabrication manner more further than the stretching approach, which is essential to provoke uniaxial oriented

chains, is expected. Influencing the piezoelectricity is also feasible by polymer thermally stretching; by this process, the phase transition from α′ to α springs, and so on, a switch from randomly oriented molecular chains to aligned chains might be achieved [24].

In helical PLA molecule chains, shear strain in the direction of the helix axis insignificantly twists the permanent bond dipoles and thus alters the polarization perpendicular to the plane of shear strain [25,26]. One of the disadvantages in this field is the PLA magnitude of piezoelectricity, which is much lower compared with most of the other PEs; solving this drawback, savants, on the one hand, inaugurated to invent hybrid biomaterials and, on the other hand, concentrated on phase transitions and stabilizing them. The convention magnitude between mechanical applied deformation and the electricity generated charge is a function of the PE constant [27].

Coming to the point, the formation of crystalline phases and its effect on d_{14} piezoelectric outcome has been presented in the previous literature, but it's the first time that the PLA 2003D is being analyzed to understand the d_{33} piezoelectric outcome of the mats. In this respect, electrospinning is considered as the best fabrication procedure to induce piezoelectricity in PLA ECM mimicking mats. The high shear force is applied to the chains which is expected to stimulate C=O dipoles to be oriented even in an amorphous structure. In fact, PLA is not a ferroelectric polymer, but it shows piezoelectricity even in amorphous state while inducing a partially long-range ordering of the chains through thermo- and/or mechanical work. The current work also explores the impact of crystallite orientation on the piezoelectric property. As a side benefit, regarding the fabrication of interconnected porous mats; in addition to what has already been denoted, a micro-aligned mat, or nanoscale fibers possess a tremendous potential to be used as artificial organs or at least a base for migration of the immature cells to the cells which are dead or can't perform their duty.

2. Materials and methods

2.1. Synthesis and post-processing

Polylactic Acid (PLA), 2003D Specific gravity ¼ 1.24; MFR g/10min (210 °C, 2.16 kg)), was received in pellet from nature-works., Minnetonka (USA). 0.68g of PLA was dissolved in a 1:4 v/v mixture of N, N- Dimethylformamide (DMF, anhydrous, ≥99.9%) and dichloromethane (DCM), respectively; both solvents were prepared from MilliporeSigma (Burlington, MA).

The polymer solution was ejected through a fine nozzle towards a substrate, often called a collector in the electrospinning (ES) process, and a large electric field was applied between the nozzle and the collector, which acted to overcome the surface tension of the polymer solution, creating a very fine jet of liquid. The jet was fast solidified as the solvent evaporates to create fibers of the polymer. These fibers may have diameters of tens to hundreds of nanometers. The high shear forces associated with the flow of solution through the nozzle can lead to significant molecular alignment in the nanofibers [28].

The ES solution flow rate was 10 ml/Hr through a 22 gauge needle (Jensen Global, Santa Barbara, CA) with 16 kV (kilovolts) applied to it, while the collector-needle distance was set

to be 7 cm. The polarized solution is then sprayed at a grounded aluminum drum, wrapped on aluminum foil, rotating at 700 rpm (rotation per minute). The experiment was conducted in a 30 ± 10% relative humidity atmosphere at ambient temperature. This results in a PLA nanofiber mat low degree of crystallinity as a matter of fast solidification.

The fibrous mat was then undergone post-processing through annealing at 105 °C for 12hr, followed by ovencooling to the room temperature. The fibrous mat was then peeled off the aluminum foil and transferred to a Teflon FEP sheet (American DURAFILM, Holliston, MA) and another FEP sheet with the weight of 120 g placed on top of the film; this sandwiching prevents the mat shrinkage, and then the sandwiched film was placed on top of a glass slide and moved inside an Oven at 150 °C for 12hr. After the complement of the process the oven was shut off and allowed to cool to the room temperature. A Complete schematic of the ES and post-processing is depicted in Fig. 2. The designed thermomechanical processing named as “two step annealing”, in fact, mimic the condition of creep regime under the constant load.

2.2. Characterization

In order to assess the electrical conductivity/resistivity of the samples before and after the post-processing, a Keithley instrument (Keithley 2601a) with an input voltage between −5 and +5 V was employed. To compare the samples' piezoelectric (PE) properties and electrical outcome, the PE Impact system was employed (PiezoTester, Functional Fibrous Materials LAB, Iran, http://ffm.aut.ac.ir) [13].

Field Emission Scanning Electron Microscopy (FESEM) was performed to visualize the orientation of the fibers. Square PLLA scaffolds with a surface of 7*7 mm^2 were mounted on a standard pin using carbon conductive tabs. The samples were then coated in gold-palladium for 1 min using a Polaron E5100 sputter coater and were imaged using an FEI Nova NanoSEM 450 at 10 kV and 12,000, 6,000, 3,000,1,500 magnifications. These studies were performed using the facilities in the school of materials science and engineering at the University of Tehran (UT).

Studying the crystalline-amorphous states and the Preferential Crystalline Planes Orientation (PCPO) in the polymeric mats was performed with a Philips PW-3710 diffractometer with Cu-Ka radiation (wavelength of k = 1.54 Å). 1-D X-ray diffraction measurements of PLA mats were carried out at room temperature using Cu Kα radiation. Patterns were recorded from 5° to 100° with a scan speed of 0.1°/min. 2-D XRD: 2D WAXD was performed to investigate the orientation of crystalline domains after ES and also in order to study the effect of post-processing. The azimuthal data was generated for these samples using XRD2D Scan v. 4.1.1. The data for each sample was then fitted with a Lorentz curve using Origin Pro 2018, and the respective Herman's Orientation Function for each sample was then calculated from these curves. The scanning rate was 1°/min with a step size of 0.1. Herman's orientation function equation is presented below:

$$F = \frac{3 < Cos^2\varphi > -1}{2} \quad (1)$$

$$< Cos^2\varphi > (hkl) = \frac{\int_0^{\frac{\pi}{2}} I(\varphi) Cos^2\varphi Sin\varphi \, d\varphi}{\int_0^{\frac{\pi}{2}} I(\varphi) \, Sin\varphi \, d\varphi} \quad (2)$$

where φ is the azimuthal angle and I(φ) is the scattered intensity along the angle φ. The orientation parameter $< Cos^2\varphi >_{(hkl)}$ has the value of unity when the normal of the reflection plane hkl is oriented parallel to the reference direction, and a value zero when the normal of the plane is perpendicular to the reference direction. By calculating Herman's orientation function, it is possible to describe the degree of the orientation of the polymeric chains between 0 and 1.

Differential Scanning Calorimetry (DSC) analysis was performed on untreated, one step annealed and two steps annealed PLA mats (sample weight: 0.6 mg) under a nitrogen purge in the temperature range of 50–210 °C and a heating rate of 10 °C/min. In order to determine the degree of crystallinity (X_c) in the course of heating, the following Eq was used:

$$Xc = 100 \times \frac{\Delta Hm - \Delta Hcc}{\Delta Hm} \quad (3)$$

where: ΔH_{cc} = cold crystallization enthalpy, ΔH_m = melting enthalpy of the sample, and ΔHm = melting enthalpy of a 100% crystalline sample. For the PLA samples, H_m^{α} was 93 J/g [29], H_m^{α} was 57 J/g [30].

The Fourier-transform infrared (FTIR) spectrum of the as-spun PLA and post proceeded samples were also obtained using a Bruker Tensor 27 spectrometer in the range of 4000–400 cm^{-1}.

3. Result and discussion

3.1. Piezoelectricity (d_{33}) of the mats

It has been demonstrated that by ES and the fabrication of micro/nanofibers, the PE performance of the non-ferroelectric materials, especially PLA, increases [31], in this way, it is essential to have smooth and thin homogenously distributed fibers with the absence of beaded regions in them, which is a result of various variables [32,33], namely; the type of solvents, the proportion of solvent and polymer, the humidity and also the atmosphere temperature, the ES applied potential and also the collector to nuzzle distance all are demonstrated in Fig. 2.

As it is depicted in Fig. 3, an appropriate selection of solvents DMF and DCM results in the formation of mostly beadles fibers, where the fibers have not been aligned because of the low number of drum rotation. As it is visible in i, j, k figures, the fibers shown some beaded regions within themselves, but annealing removes these highly amorphous regions, and as it is depicted in the median, f, g, and h SEM figures, of the one step annealed samples and of course the upper column of two steps annealed samples, the beaded regions are cleared

away. The post-processing operation actually causes an increase in fiber diameters and also their alignment, as depicted in Fig. 3d and e.

As it is obvious in Fig. 4, the piezoelectricity has been increased through post-processing treatment slightly by one step annealing at 105 °C and dramatically by two step annealing at 150 °C (up to 3 times higher than the just spun samples). The issue which is in the course of attention is the root of this promotion and is going to be answered in the following sections. As it is claimed by Zhao et al. [34], each fiber PE outcome is about 3.1 pc/N, and it is possible to hypothesis that the low PE outcome of these patches is based on the misaligned fibers that cancel out each other piezo property in comparison to amplification.

3.2. Phase transition behavior

First of all, it is essential to investigate the effect of the thermal process on polymer chains and bondings; to make it clear the FTIR results are projected in Fig. 5. The important peaks of C=O as the source of piezoelectricity and other bonds have not changed in one step or two steps annealed process. Two small bands at 921 cm^{-1} and 955 cm^{-1} are ascribed to a 10_3 helix sensitive crystallization band and amorphous structure, respectively. In the α phase, the carbonyl stretching vibrations bands showed a complex splitting pattern at 1776, 1759, and 1749 cm^{-1}. In the α′ phase PLA film, the carbonyl stretching vibrations bands had only a single peak at 1759 cm^{-1}. The same results have been reported in [35,36]. Differential Scanning Calorimetry (DSC) was used to investigate the crystallinity percentage of the semicrystalline PLA polymer. The crystallinity percentage is determined to be induced by any thermal process, including annealing and also thermo-mechanical process. It is proved that the promotion of the crystallinity percentage effectively promotes the PE properties [15].

Micro/nanoscale piezoelectricity measurements are attainable by advanced characterization techniques [37]. For instance, Smith et al. inscribed the determination of shear piezoelectricity in extremely oriented PLLA nanowires, which were also extremely crystalline, the interpreted result terminated an advance in the degree of crystallinity up to 70%, using PE Force Microscopy (PFM), the estimated d14 PE coefficient was about 8 pC/N [37].

As it is apparent in Fig. 6, from the just spun samples to the two steps annealed patches, the crystallinity percentage shows an increasing trend. The matter of crystalline structure in polymers arises from the alignment of chains, and the chain relaxation is much faster than chain extension at ES conditions, which results in the most amorphous structure of the as-spun sample, as is tangible in Fig. 6b. The α crystalline diffraction peaks of 1D-XRD which are formed at a temperature above 120 °C, appear at 2θ values of 16.7°, 19.1°, 22.4° corresponding to Miller indices for planes 200/110, 203, 015, respectively. However, the 1D-XRD diffraction peaks of α' crystalline phase, which is induced from an amorphous state at temperatures below the 120 °C, appear at 2θ values of 16.4°, 18.7°, corresponding to 200/110, 203 planes, respectively. It is difficult to distinguish both phases based on XRD patterns because of their similarity in conformation [5,23]. In this respect, Table 1 provides comprehensive detail on PLA conformation, crystalline phase formation, and the condition [5,23,38].

While taking the DSC results into consideration; the XRD results suggest the formation of crystalline states of α and α'. It is evident that two steps of annealing result in the construction of α crystalline phase with the highest crystallinity percentage after 12 h exposing to creep regime (under the constant load) at 150 °C. In contrast, thermal processing below the transition temperature at 105 °C and the same annealing time without loading forms both of the α, and α′ phases. The formation of these two crystalline states originates from the time of thermal processing, which was long enough for the transformation of α′ to α phase. It has been mentioned in the literature that crystalline transformation from α′ to α is a type of disorder to order phase transformation [30,39]. In order to supply an adequate viewpoint to both of the phases' crystalline states, considering their state in fibers and the transition between them respecting all the details of the crystalline state and the conformation of the chains, Fig. 7 is provided. Further description is provided in figure's caption.

3.3. Texturization

Philips PW-3710 diffractometer was employed to illustrate the development of chain conformation in the crystalline phase. Annealing the material increases the order of the polymer chains, thus inhibiting dipole rotation and promoting the ferroelectric and PE properties of the material as an impact of the most thermodynamically stable state [43]. Annealing does not necessarily generate anisotropy and often acts to reduce it. Therefore, heat treatment alone is not a sufficient condition to ensure the PE properties of a polymer are expressed.

Calculating Herman's orientation function is an effective procedure to obtain the degree of chain alignment. As the chains get aligned in a higher-order manner, Herman's orientation function would be closer to 1, and vice versa; the 0 calculated number would mean the inhomogeneously directed chains. Herman's orientation function represents polymer-chain orientation for systems with fiber symmetry (uniaxial orientation) and the Herman's-Stein orientation factors express uniaxial orientation for each of the crystallographic axes of crystalline polymers [44]. The calculated Herman's orientation factors, in the present case, are presented in Fig. 8a. Here below, we are going to discuss Herman's orientation factors higher than 0.3 because of the fact that the numbers lower than that have an inferior proportion of crystallites. On the one hand, as it is depicted, the chain alignment in the one-step annealed structure, has been led to the formation of 110 crystalline planes, either originated from the α′ or α phases. The calculated Heramn's orientation function has appeared having a number close to 0.48 in the range of 75–125 which denotes a high crystal rotation in this mentioned scope. On the other hand, Herman's orientation function of the two steps annealed structure possess higher values ranging between 220 and 310.

To pave the way for understanding the evolution of Herman's orientation function, distribution of the preferential crystal orientation plane for one step and two step annealed scaffolds, are depicted in Fig. 8b, d and Fig. 8c, e, respectively. It can be concluded from the 3D graphs that the absence of peaks results into a low or zero values of Herman's orientation function. The intensity values represent the number of crystals aligned to a specific angle. In one-step annealed mats, the intensity is lower in comparison to the two

steps annealed patches. This means that the preferential crystal orientation planes have been randomly oriented through one step annealing while it is going to be more texturized in two steps annealed samples. Herman's orientation functions are also higher in the case of one-step annealed condition, which is literally originated from the fact that crystals have not been aligned but are randomly oriented, i.e., the crystallites have been formed in various directions.

It should be denoted that the PLA patterns don't represent a cloudy pattern of the amorphous structure [45,46] as well as representing an adapted scattering direction just related to the specified distribution of 110 planes [47]. As it is being tried to be well described, the two steps annealed structure have been strongly texturized, and most of the crystallites have been located approximately near the transverse direction (TD), that is to say, the normal direction of the 110 planes is perpendicular to the electrospinning direction. In this regard, it can be claimed that the crystallites have been formed aligned with the fibers direction. It can be concluded that annealing has the potential to cause a phase transformation, but the thermo-mechanical processing actually helps the crystal rotation of the chains within the fibers (2D-WAXD patterns in Fig. 8b, c, d, and e show the anisotropy of (200/110) planes and the preferential crystal orientation).

The results indicate that the preferential orientation of the normal direction of 110 crystalline planes aligned with transvers direction. The annealing would cause such high anisotropy, however, it can be related to the creep-induced crystallization form α' disordered crystalline structure to αcrystalline ordered structure [30,48]. During the thermomechanical processing, the amorphous chains gradually reorient in the plane of the fibers, and cause disappearing the randomly oriented halo. This type of texturization, in the absence of other higher-order peaks, represents the threedimensional crystalline order has been relatively well established.

Taking the hole intensities in various directions in mind, low intensity diffracted peaks along the RD and TD do not exhibit well-developed crystalline regions. This behavior is due to the random orientation of the chain segments in the fiber plane. Thus they have a low chance to form in parallel pattern with each other and crystallize. Still, it is worth mentioning that the processing temperature was high enough to form a type of crystalline structure, actually in the direction of TD, up to a ratio of 59%, and it can be concluded that the crystallites are formed along the TD partially parallel to each other causing a promoted piezoelectric outcome.

4. Conclusion

In this paper, the PLA scaffolds d_{33} piezo constant for the first time and its promotion regarding the crystallization induced through thermo-mechanical processing was measured. Annealing at 105 °C for 12 h resulted in the formation of both the disordered-α' and ordered-α crystalline phases by the crystallinity percentage of 20% and 27%, respectively; a total crystallinity percentage of 47%. Creep-induced crystallization at 150 °C for 12 h was investigated, it resulted in the formation of the α phase holding higher crystallinity of about 59%. It was concluded that any thermal process above the cold crystallization temperature induced an appreciable crystallinity percentage up to 59%. Analyzing Herman's orientation

function and texture evolution showed that the one-step annealing provided an appropriate condition for randomly oriented crystallites. In contrast, two steps of annealing resulted in a more texturized microstructure along the electrospinning direction. In one step annealed samples, piezoelectricity did not show a sharp increasing trend in comparison to un-treated scaffolds, while texturization in two steps-annealed patches caused a dramatic promotion of the d_{33} piezoelectric value from 0.078 fc/N to 0.21fc/N.

Declaration of Competing Interest

Part of the research reported in this paper was supported by National Institute of Dental & Craniofacial Research of the National Institutes of Health under award number R15DE027533, 1R56 DE029191-01A1 and 3R15DE027533-01A1W1. The content is solely the responsibility of the authors and does not necessarily represent the official views of the National Institutes of Health.

REFERENCES

[1]. Tang P, Song P, Peng Z, Zhang B, Gui X, Wang, et al. Chondrocyte-laden GelMA hydrogel combined with 3D printed PLA scaffolds for auricle regeneration. Mater Sci Eng C 2021;130:112423. 10.1016/j.msec.2021.112423.

[2]. Review FC. Piezoelectric polymers : theory, challenges and opportunities. Int Mater Rev 2021:1–24. 10.1080/09506608.2021.1915935.

[3]. Ito S, Imoto K, Takai K, Kuroda S, Kamimura Y, Kataoka, et al. Sensing using piezoelectric chiral polymer fiber. Jpn J Appl Phys Sep. 2012;51:09LD16. 10.1143/jjap.51.09ld16.

[4]. Tian Zheng MJH, Yue Zhilian, Wallace Gordon G, Du Yi, Zheng T, Yue Z, et al. Nanoscale piezoelectric effect of biodegradable PLA-based composite fibers by piezoresponse force microscopy. Nanotechnology May 2020. 10.1088/1361-6528/ab96e3.

[5]. Zhang Z, Wang X, Wang Y, Shen C, Liu C, Wang Z. Melt extension-induced shish-kebabs with heterogeneous spatial distribution of crystalline polymorphs in lightly crosslinked poly(lactic acid). Polymer 2020;208:122875. 10.1016/j.polymer.2020.122875.

[6]. Chen J, Rong C, Lin T, Chen Y, Wu J, You J, et al. Stable Co-continuous PLA/PBAT blends compatibilized by interfacial stereocomplex crystallites: toward full biodegradable polymer blends with simultaneously enhanced mechanical properties and crystallization rates. Macromolecules Mar. 2021;54(6):2852–61. 10.1021/acs.macromol.0c02861.

[7]. Ou X, Cakmak M. Influence of biaxial stretching mode on the crystalline texture in polylactic acid films. Polymer 2008;49(24):5344–52. 10.1016/j.polymer.2008.09.053.

[8]. Li Z, Ye L, Zhao X, Coates P, Caton-Rose F, Martyn M. Structure and biocompatibility of highly oriented poly(lactic acid) film produced by biaxial solid hot stretching. J Ind Eng Chem 2017;52:338–48. 10.1016/j.jiec.2017.04.008.

[9]. Meaurio E, Martinez De Arenaza I, Lizundia E, Sarasua JR. Analysis of the C=O stretching band of the a-crystal of poly(L-lactide). Macromolecules 2009;42(15):5717–27. 10.1021/ma9008109.

[10]. Li B, Hu X, Zhang Q, Peng X, Xiang Y. Improved piezoelectricity of polylactide using vitamin B2 for poling-free mechanical and acoustic nanogenerators. J Mater Sci 2021;56(1):902–12. 10.1007/s10853-020-05283-1.

[11]. Li X, Chen S, Zhang X, Li J, Liu H, Han N, et al. Poly-l-Lactic acid/graphene electrospun composite nanofibers for wearable sensors. Energy Technol 2020;8(5):1901252. 10.1002/ente.201901252.

[12]. Wang C, Yue H, Huang W, Lin X, Xie X, He Z, et al. Cryogenic 3D printing of heterogeneous scaffolds with gradient mechanical strengths and spatial delivery of osteogenic peptide/{TGF}-$upbeta$1 for osteochondral tissue regeneration. Biofabrication Mar. 2020;12(2):25030. 10.1088/1758-5090/ab7ab5.

[13]. Azmi S, Varkiani S-MH, Latifi M, Bagherzadeh R. Tuning Energy harvesting devices with different layout angles to robust the mechanical-to-electrical energy conversion performance. J Ind Textil 2020:1528083720928822. 10.1177/1528083720928822.

[14]. Ando M, Kawamura H, Kageyama K, Tajitsu Y. Film sensor device fabricated by a piezoelectric poly(L-lactic acid) film. Jpn J Appl Phys Sep. 2012;51:09LD14. 10.1143/jjap.51.09ld14.

[15]. Curry EJ, Le TT, Das R, Ke K, Santorella EM, Paul D, et al. Biodegradable nanofiber-based piezoelectric transducer. Proc Natl Acad Sci USA Jan. 2020;117(1):214–20. 10.1073/pnas.1910343117. [PubMed: 31871178]

[16]. Jean-Mistral C, Basrour S, Chaillout J-J. Comparison of electroactive polymers for energy scavenging applications. Smart Mater Struct Jul. 2010;19(8):85012. 10.1088/0964-1726/19/8/085012.

[17]. Smith M, Kar-Narayan S. Piezoelectric polymers: theory, challenges and opportunities. Int Mater Rev 2021:1–24. 10.1080/09506608.2021.1915935.

[18]. De Santis P, Kovacs AJ. Molecular conformation of poly(S-lactic acid). Biopolymers 1968;6(3):299–306. 10.1002/bip.1968.360060305. [PubMed: 5641931]

[19]. Pan P, Zhu B, Kai W, Dong T, Inoue Y. Polymorphic transition in disordered poly(l-lactide) crystals induced by annealing at elevated temperatures. Macromolecules Jun. 2008;41(12):4296–304. 10.1021/ma800343g.

[20]. Sapra R, Verma RP, Maurya GP, Dhawan S, Babu J, Haridas V. Designer peptide and protein dendrimers: a cross-sectional analysis. Chem Rev Nov. 2019;119(21):11391–441. 10.1021/acs.chemrev.9b00153.

[21]. Heeley EL, Billimoria K, Parsons N, Figiel Ł, Keating EM, Cafolla CT, et al. In-situ uniaxial drawing of poly-L-lactic acid (PLLA): following the crystalline morphology development using time-resolved SAXS/WAXS. Polymer 2020;193:122353. 10.1016/j.polymer.2020.122353.

[22]. Shin DM, Hong SW, Hwang YH. Recent advances in organic piezoelectric biomaterials for energy and biomedical applications. Nanomaterials 2020;10:1. 10.3390/nano10010123.

[23]. Cocca M, Di Lorenzo ML, Malinconico M, Frezza V. Influence of crystal polymorphism on mechanical and barrier properties of poly(l-lactic acid). Eur Polym J 2011;47(5): 1073–80. 10.1016/j.eurpolymj.2011.02.009.

[24]. Yoshida T, Imoto K, Tahara K, Naka K, Uehara Y, Kataoka S, et al. Piezoelectricity of poly(L-lactic acid) composite film with stereocomplex of poly(L-lactide) and poly(D-lactide). Jpn J Appl Phys Sep. 2010;49(9):09MC11. 10.1143/jjap.49.09mc11.

[25]. Fukada E Recent developments of polar piezoelectric polymers. IEEE Trans Dielectr Electr Insul 2006;13(5):1110–9. 10.1109/TDEI.2006.247839.

[26]. Ando M, Kawamura H, Kitada H, Sekimoto Y, Inoue T, Tajitsu Y. Pressure-sensitive touch panel based on piezoelectric poly(L-lactic acid) film. Jpn J Appl Phys Sep. 2013;52(9S1):09KD17. 10.7567/jjap.52.09kd17.

[27]. Rampal A, Kleiman RN. Optical actuation of a micromechanical photodiode via the photovoltaic-piezoelectric effect. Microsystems Nanoeng. 2021;7(1):29. 10.1038/s41378-021-00249-y.

[28]. Richard-Lacroix M, Pellerin C. Molecular orientation in electrospun fibers: from mats to single fibers. Macromolecules Dec. 2013;46(24):9473–93. 10.1021/ma401681m.

[29]. Pereira RB, Morales AR. Estudo do comportamento térmico e mecânico do PLA modificado com aditivo nucleante e modificador de impacto. Polímeros - Ciência Tecnol 2014;24(2): 198–202. 10.4322/polimeros.2014.042.

[30]. Zhang J, Tashiro K, Tsuji H, Domb AJ. Disorder-to-Order phase transition and multiple melting behavior of poly(l-lactide) investigated by simultaneous measurements of WAXD and DSC. Macromolecules Feb. 2008;41(4):1352–7. 10.1021/ma0706071.

[31]. Cuong NT, Barrau S, Dufay M, Tabary N, Da Costa A, Ferri A, et al. On the nanoscale mapping of the mechanical and piezoelectric properties of poly (L-lactic acid) electrospun nanofibers. Appl Sci 2020;10(2). 10.3390/app10020652.

[32]. Smyth M, Poursorkhabi V, Mohanty AK, Gregori S, Misra M. Electrospinning highly oriented and crystalline poly(lactic acid) fiber mats. J Mater Sci 2014;49(6):2430–41. 10.1007/s10853-013-7899-z.

[33]. Haider A, Haider S, Kang IK. A comprehensive review summarizing the effect of electrospinning parameters and potential applications of nanofibers in biomedical and biotechnology. Arab. J. Chem 2018;11(8):1165–88. 10.1016/j.arabjc.2015.11.015.

[34]. Zhao G, Huang B, Zhang J, Wang A, Ren K, Wang ZL. Electrospun poly(l-lactic acid) nanofibers for nanogenerator and diagnostic sensor applications. Macromol Mater Eng 2017;302(5):1600476. 10.1002/mame.201600476.

[35]. Shao J, Chen C, Wang Y, Chen X, Du C. Early stage evolution of structure and nanoscale property of nanofibers in thermally induced phase separation process. React Funct Polym 2012;72(10):765–72. 10.1016/j.reactfunctpolym.2012.07.011.

[36]. Kalish JP, Aou K, Yang X, Hsu SL. Spectroscopic and thermal analyses of α′ and α crystalline forms of poly(l-lactic acid). Polymer 2011;52(3):814–21. 10.1016/j.polymer.2010.12.042.

[37]. Sencadas V, Ribeiro C, Heredia A, Bdikin IK, Kholkin AL, Lanceros-Mendez S. Local piezoelectric activity of single poly(L-lactic acid) (PLLA) microfibers. Appl Phys A 2012;109(1):51–5. 10.1007/s00339-012-7095-z.

[38]. Flaig F, Ragot H, Simon A, Revet G, Kitsara M, Kitasato L, et al. Design of functional electrospun scaffolds based on poly(glycerol sebacate) elastomer and poly(lactic acid) for cardiac tissue engineering. ACS Biomater Sci Eng Apr. 2020;6(4):2388–400. 10.1021/acsbiomaterials.0c00243. [PubMed: 33455317]

[39]. Cartier L, Okihara T, Ikada Y, Tsuji H, Puiggali J, Lotz B. Epitaxial crystallization and crystalline polymorphism of polylactides. Polymer 2000;41(25):8909–19. 10.1016/S0032-3861(00)00234-2.

[40]. Wasanasuk K, Tashiro K. Crystal structure and disorder in Poly(l-lactic acid) δ form (α′ form) and the phase transition mechanism to the ordered α form. Polymer 2011;52(26):6097–109. 10.1016/j.polymer.2011.10.046.

[41]. Lotz B Crystal polymorphism and morphology of polylactides. Adv Polym Sci 2018;279:273–302. 10.1007/12_2016_15.

[42]. Meaurio E, Zuza E, López-Rodríguez N, Sarasua JR. Conformational behavior of poly(L-lactide) studied by infrared spectroscopy. J Phys Chem B 2006;110(11):5790–800. 10.1021/jp055203u. [PubMed: 16539526]

[43]. Liu S, Cui Z, Fu P, Liu M, Zhang L, Z. Li, et al. Ferroelectric behavior and polarization mechanism in odd-odd polyamide 11,11. J Polym Sci Part B Polym Phys 2014;52(16):1094–9. 10.1002/polb.23537.

[44]. White JL, Spruiell JE. The specification of orientation and its development in polymer processing. Polym Eng & Sci 1983;23(5):247–56. 10.1002/pen.760230503.

[45]. and S. C. Piyawanee Jariyasakoolroj, Kohji Tashiro, Wannee Chinsirikul, noppadon kerddonfag, “Microstructural analyses of biaxially oriented polylactide: modified thermoplastic starch film with drastic improvement in Toughness.pdf.” .

[46]. Bébin P, Prud'Homme RE. Effect of comp drif. J Polym Sci Part B Polym Phys 2001;39(1):2363–77. 10.1002/polb.0000.

[47]. Ding S, Fang C, Wang X, Wang Z. Crystallization-driven microstructure changes during microphase separation for environment-friendly thermoplastic triblock copolymer elastomers. Polymer 2020;186:121993. 10.1016/j.polymer.2019.121993.

[48]. Nouri S, Lafleur PG, Dubois C. Enhanced film blowing of polylactide by incorporating branched chains and stereocomplex crystals. Int Polym Process 2015;30(4):500–10. 10.3139/217.3080.

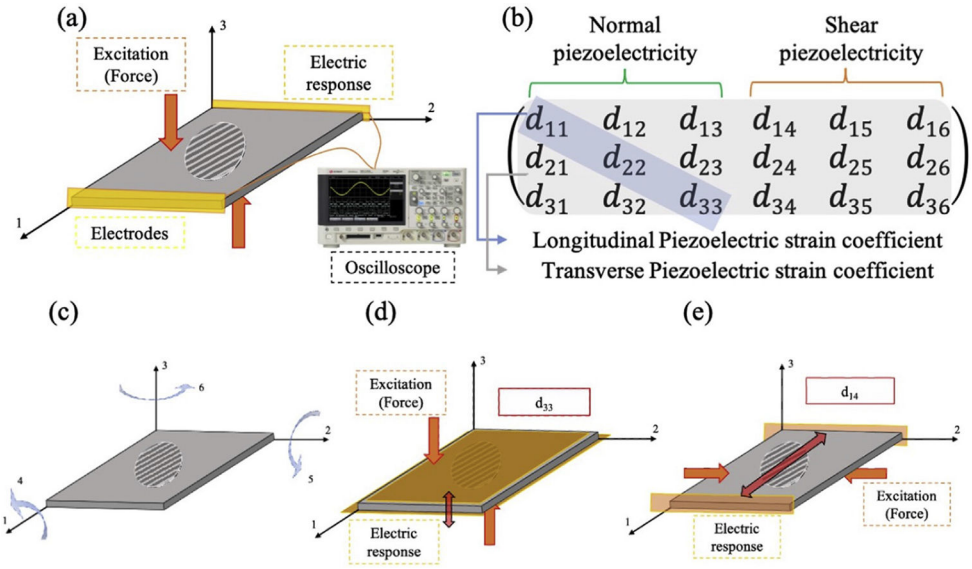

Fig. 1.

(a) Relationship between applied normal (σ) and shear (τ) stress and corresponding induced electric field (E), (b) piezoelectricity matrix, (c) an illustration of normal and shear directions, (d) d33 as an example of normal-longitudinal PE response, (e) d14 as an example of shear-longitudinal PE response.

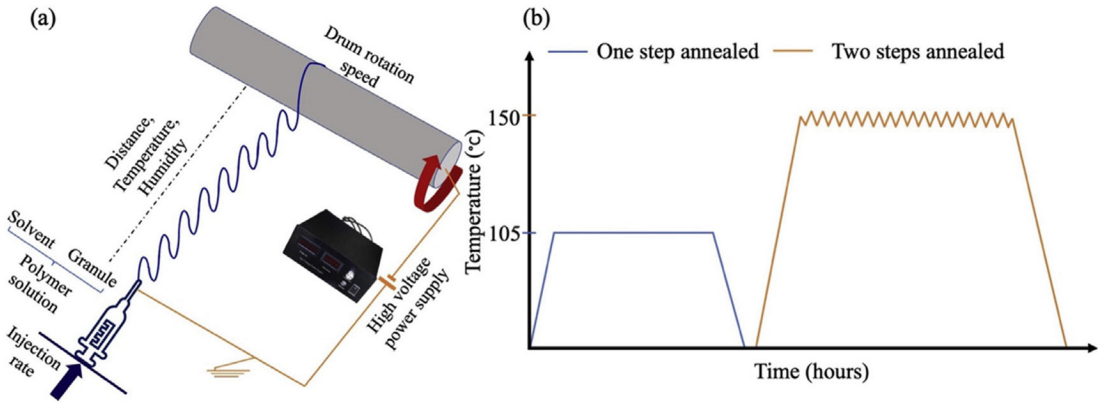

Fig. 2.

(a) Electrospinning variables and process (b) the post-processing procedure applied to the polymeric PLA mats, each of the post-processing have taken along 12 h.

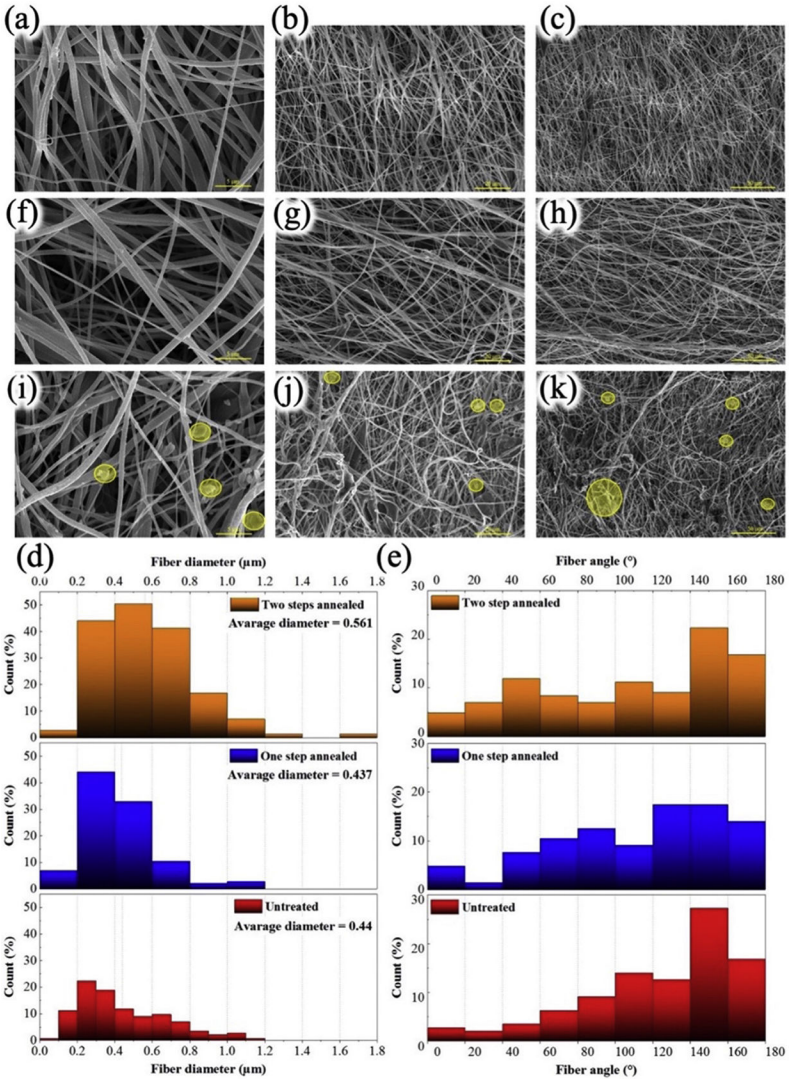

Fig. 3.

(a, b, c) FESEM picture of two steps annealed samples, scale bar: 5, 20, and 50 µm respectively (f, g, h) FESEM picture of one-step annealed mats, scale bar: 5, 20, and 50 mm respectively (i, j, k) FESEM picture of as-spun scaffolds, scale bar: 5, 20, and 50 mm respectively, (d) Fiber diameter dispersion with their proportion, related to as-spun, one step annealed and two steps annealed from lower box to top respectively, (e) The degree of fiber alignment with their proportion, related to just spun, one step annealed and two steps annealed from lower box to top respectively.

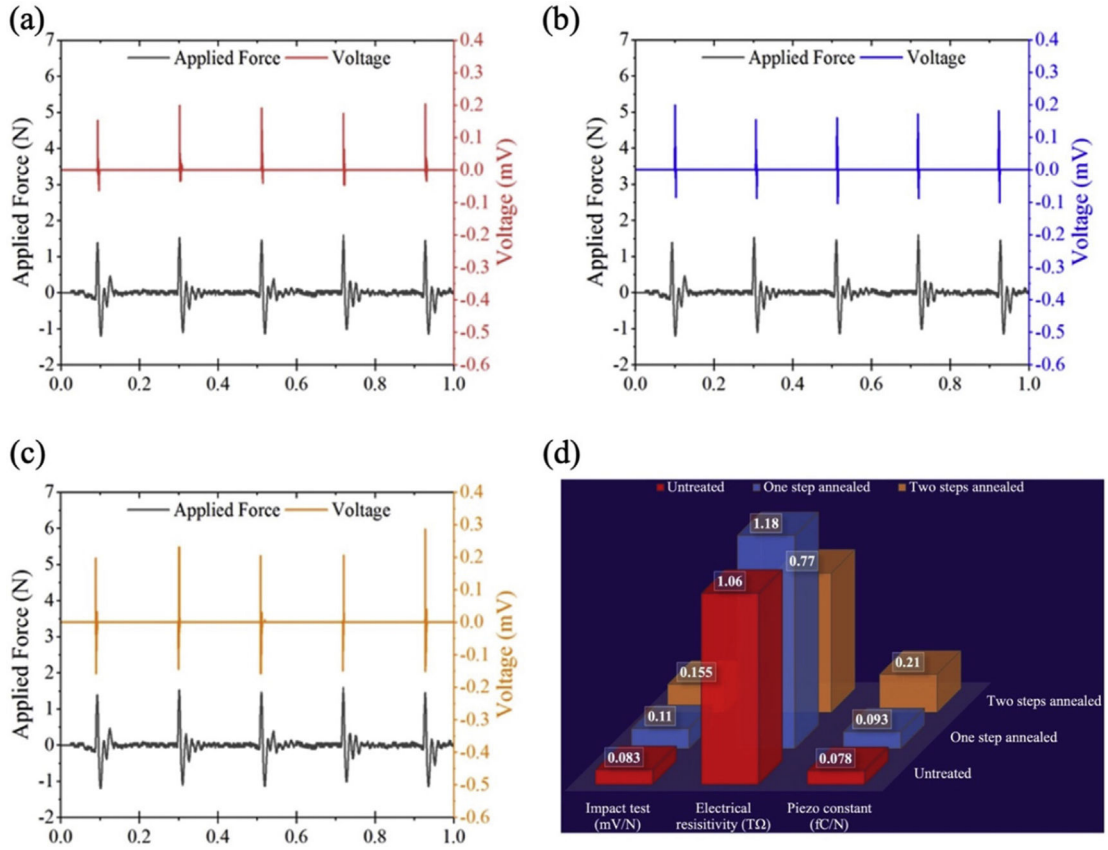

Fig. 4.

(a) Untreated (as spun) PLA mat impact test result, (b) one step annealed PLA mat impact test outcome, (c) Two steps annealed PLA impact test termination, (d) schematic of the impact test outgrowth, samples Electrical resistivity and the value of d_{33}.

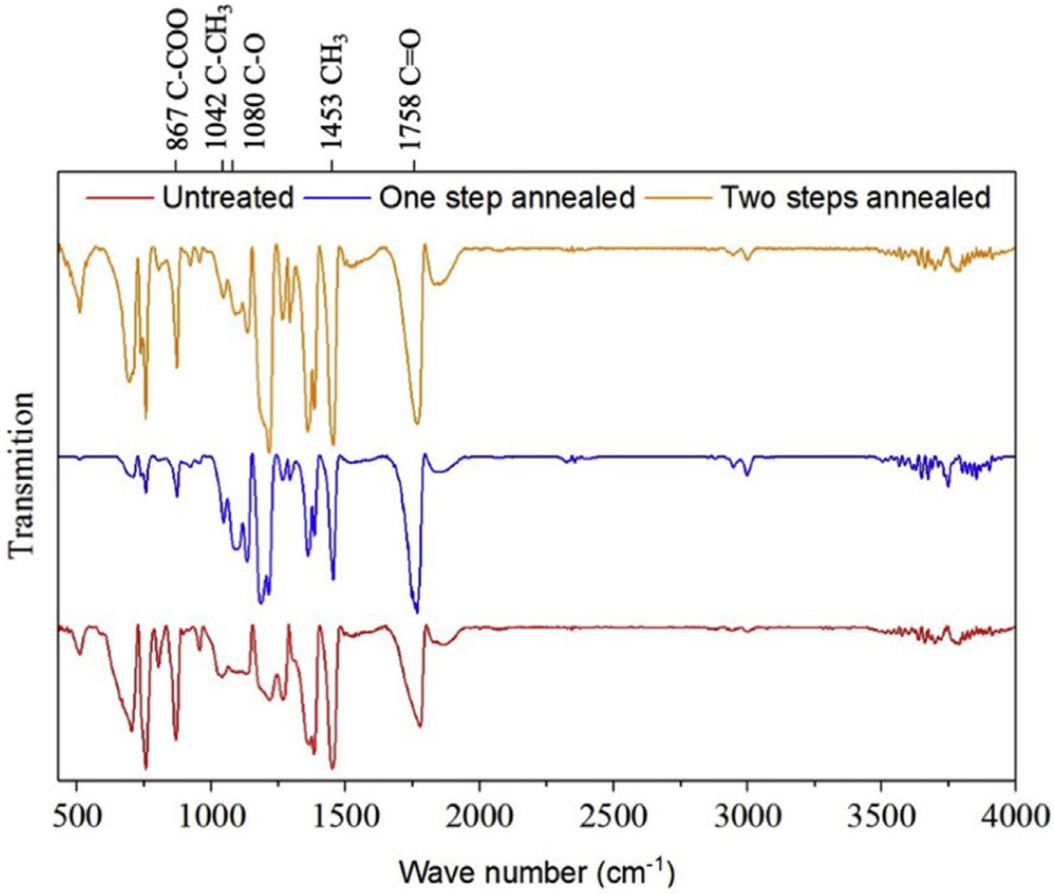

Fig. 5.
The FTIR results of As-spun, One step annealed, and Two steps annealed patches.

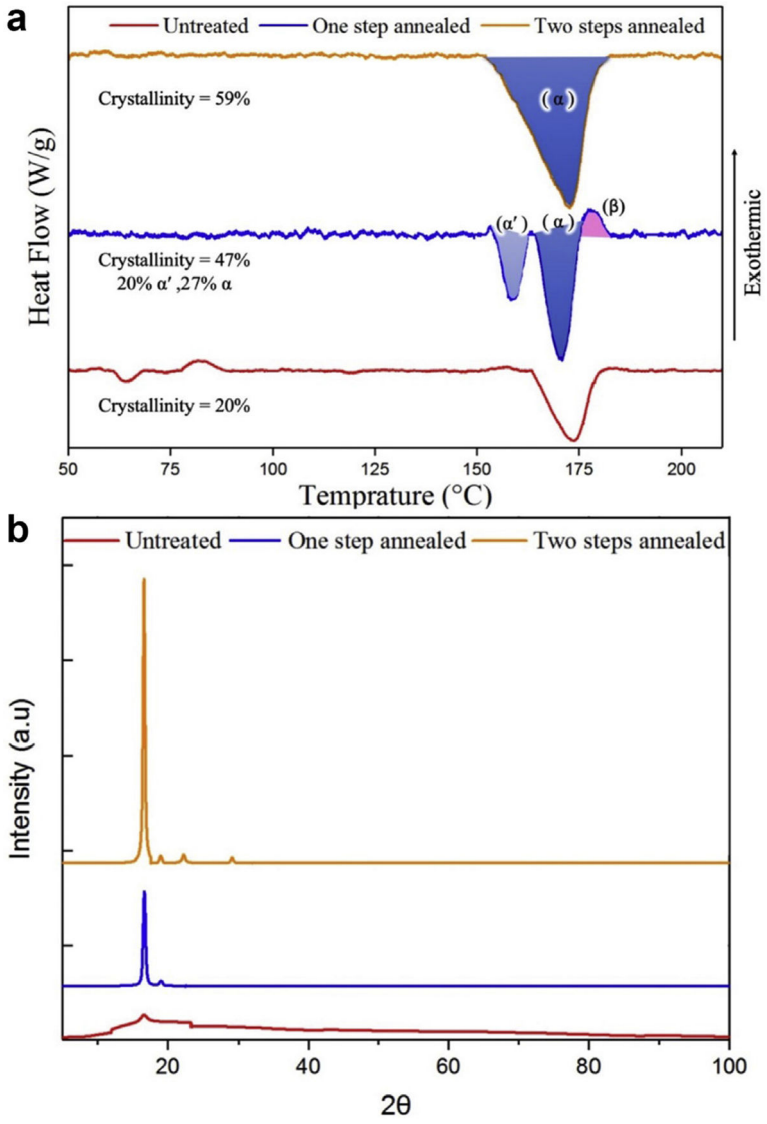

Fig. 6.

(a) DSC results of the patches regarding their crystallinity percentage and also denoting the crystalline phases, (b) 1D-XRD results demonstrating that the crystalline phases have been induced by the further thermo-mechanical process.

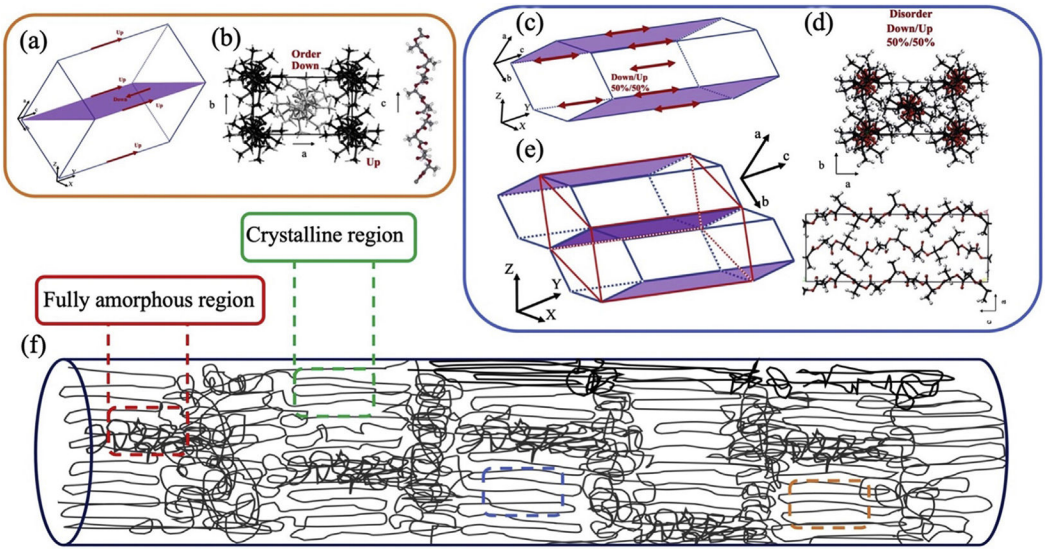

Fig. 7.

(a) Orthorhombic PLA- α crystalline phase, (b) the sequence of chain alignment in the α-order crystalline phase, (c) pseudo-hexagonal PLA- α′ crystalline phase, (d) the sequence of chain alignment in the α′-disorder crystalline phase, (e) spatial imagination which leads to understanding the formation of an orthorhombic structure by juxtaposing two pseudo-hexagonal unit cells, (f) A single fiber containing lots of aligned/unaligned chains within itself, the aligned regions form the crystalline parts while unaligned regions are attributed to the amorphous divisions [40-42].

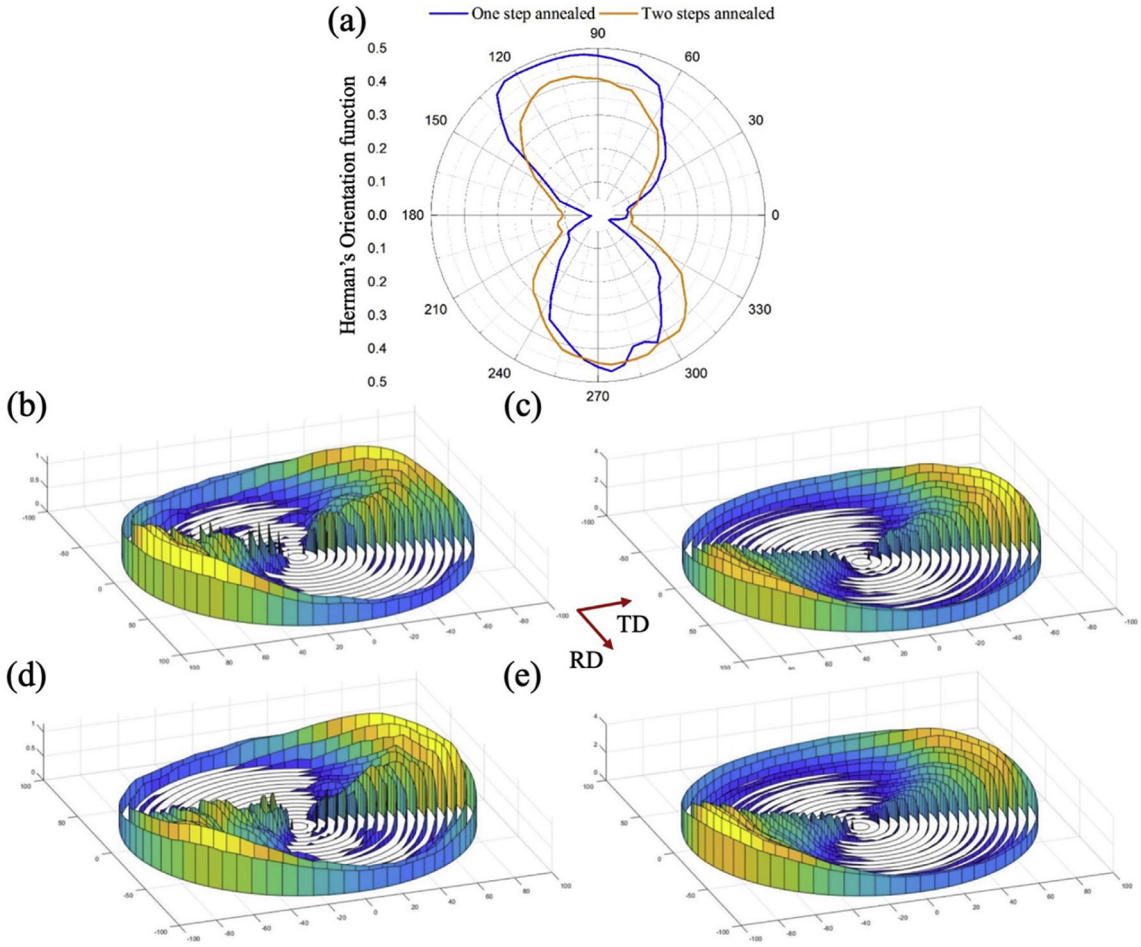

Fig. 8.

(a) Herman's orientation Function distribution of one step and two steps annealed patches (b) The 110 plane distribution of one step annealed (c) and two steps annealed (d) patches in various crystal rotation from 0 to 90°. (d) and (e) are another schematic of (b) and (c) which has been rotated 180°.

Table 1

Various PLA crystalline phases regarding their unit cell parameters, their chains conformation state, and formation condition.

Crystalline phase	Unit cell	Conformation	Formation condition
α	Orthorhombic a = 9.95 °A, b = 6.25 °A, c = 8.8 °A	103 left-handed helix	Crystalizes above 120 °c
α′	Pseudo-hexagonal a = b = 6.2 °A, c = 28.8 °A	103 distorted helix	Crystalizes below 120 °c
β	Trigonal a = b = 10.52 °A, c = 8.8 °A	31 left-handed helix with frustrated structure	Drawing ratio ≥6 T ≈ $T_{melting}$
γ	Orthorhombic a = 9.95 °A, b = 6.25 °A, c = 8.8 °A	31 antiparallel left-handed helix	Epitaxial crystallization on hexamethylbenzene (HBM) substrate